Proceedings World Geothermal Congress 2020+1
Reykjavik, Iceland, April - October 2021

Modeling and Analysis of Multiple Hydraulic Fracturing Design in EGS

Dharmendra Kumar and Ahmad Ghassemi

100 Boyd St., Mewbourne School of Petroleum and Geological Engineering

kumar_dharmendra@ou.edu; ahmad.ghassemi@ou.edu

Keywords: Enhanced geothermal systems, stress shadowing effect, conventional zipper fracturing, modified zipper fracturing, displacement discontinuity method.

ABSTRACT

The paper presents three-dimensional numerical simulations of multiple fracture propagation from horizontal wells in enhanced geothermal systems. The multistage hydraulic fracturing of horizontal wells is commonly used stimulation technique to enhance the permeability of unconventional reservoirs in the oil and gas industry. However, a detailed study of applicability and design requirements for multistage fracturing of the EGS wells is required. In this work, we use "GeoFrac-3D" which is a 3D hydraulic fracture propagation model with advanced capabilities to simulate multistage fracturing of the horizontal wells. Numerical examples of multiple horizontal wells stimulation using conventional and modified zipper fracturing are presented the U.S. Department of Energy's FORGE (Frontier Observatory for Geothermal Energy) well(s). The parameters controlling the fracture geometry, upward growth and fracture interactions are investigated. Conditions for planar and nonplanar growth and potential network complexity are studied. The heat exchange areas and potential flow paths for various designs are illustrated. The parameters controlling the fracture geometry, upward growth and fracture interactions are investigated. The results demonstrate the fracturing fluid density can play a role in preventing upward growth of the fractures and can in fact, promote downward growth. Results also show that hydraulic fracture in both the conventional and modified zipper fracturing techniques can coalesce at their tips, which increases chances of wells connectivity through fracture-to-fracture interference. The modified zipper fracturing generates more complex fracture network, with potentially more surface area.

1. INTRODUCTION

Low permeability hot rocks provide a substantial source for geothermal energy which can be extracted using the enhanced or engineered geothermal systems (EGS) concept, where energy is recovered by circulation of water through natural or man-made hydraulic fracture networks. Therefore, cracks and fractures have a significant role in the extraction of geothermal energy by providing the major pathways for fluid flow and heat exchange. In the absence of natural fractures or adequate connectivity, a fracture network can be created using hydraulic fracturing. To enhanced contact area for water circulation, multiple fracturing is preferred instead of a single long fracture. Often, multiple fractures are created by stimulating multiple horizontal wells either in simultaneous or sequential "zipper" fracturing technique (Waters et al., 2009; Sesetty and Ghassemi, 2015; Kumar and Ghassemi, 2016). Zipper fracturing with an initial offset between fractures from the two wells is referred to as "modified zipper" fracturing (MZF). The mechanical interaction among multiple propagating fractures is an important issue to be considered in the multiple fracture design. The mechanical interaction between multiple fractures is caused by "stress shadowing" effect. The term stress shadow represents variation of stresses in the region surrounding a fracture. If a second hydraulic is created in the vicinity of (often parallel to) an existing opened fracture, the second fracture could experience a stress greater than the original in-situ stress. As a consequence, a higher fluid pressure would be required to propagate the second fracture and its growth and trajectory could be impacted. The spacing between the fractures, and the in-situ stress contrast play an important role in the mechanical interaction of multiple hydraulic fractures (Sesetty and Ghassemi, 2013; Kumar and Ghassemi, 2016 and 2018). Estimation of the optimal fracture spacing is a critical issue for multiple fracturing which in also influenced by thermal interference among the fractures for EGS applications. To avoid the thermal interference among fractures, the lateral wells must be separated by at least twice the thermal diffusion distance ($\sqrt{c.t}$) and distance between fracture must be greater than this thermal diffusion distance, where c and t are the rock thermal diffusivity and operation periods, respectively.

In this work, a 3D fully coupled numerical model "GeoFrac-3D" for the hydraulic fracture simulation is developed using a combination of the displacement discontinuity (DD) method for the rock mass deformation and the finite element method for the fluid flow modeling. The fracture propagation is implemented in the framework of the linear elastic fracture mechanic approach. The fracturing fluid is assumed incompressible and follows the Newtonian behavior. The rock matrix is assumed linear elastic, homogeneous, and isotropic with constant physical properties. Details of mathematical formulations and methodology for numerical implementation are presented first. Finally, numerical examples of multi-lateral well fracturing the U.S. Department of Energy's Utah FORGE site are presented.

2. THEORY AND GOVERING EQUATIONS

2.1 Deformation of Solid Rock Matric and Fractures

The problem of multiple interacting fractures in elastic rock needs be treated numerically. An effective technique is the displacement discontinuity (DD) method, which is an indirect boundary element method (BEM). The DD method is based on the fundamental solution of the stress-strain relation of an infinite elastic medium. It is assumed that a discrete approximation of a continuous distribution of the DD can be made along a fracture surface. The concept of the DD was extensively developed by Crouch and Starfield (1983) using the line element with constant strength formulation for an infinite elastic medium for 2D and 3D problems. Later authors (see, Wiles and Curran, 1982; Vandamme and Curran, 1989; Ghassemi and Roegiers, 1996) developed 3D displacement discontinuity formulation based on the Green's functions in an infinite, and elastic media for a point source, which can be applied to the fracture of any arbitrary shape in 3D space. Based on the point load DD solutions, the induced stresses (σ_{ij}) at a field point $\mathbf{x} = (x, y, z)$ due to concentrated point source of the DD at any source point $\mathbf{x}' = (x', y', z')$ are given as (Vandamme and Curran, 1989):

$$\sigma_{ij}(\mathbf{x}) = S_{ijkn}(\mathbf{x}, \mathbf{x'}) \cdot D_{kn}(\mathbf{x'}) \tag{1}$$

where S_{ijkn} are the stress kernels for 3D elasticity case, which are defined based on the Green's functions as listed in Vandamme and Curran (1989), and D_{kn} represents displacement discontinuity vector. For three-dimensional elasticity problems, vector D_{kn} will have one normal component (D_n) and two shear components (D_{s1} and D_{s2}). For total effects of the fracture opening and shear rides, the fundamental solutions need to be integrated over the fracture surface (A) as:

$$\sigma_{ij}(\mathbf{x}) = \int\int_A S_{ijkn}(\mathbf{x}, \mathbf{x'}) \cdot D_{kn}(\mathbf{x})\, dA \tag{2}$$

The above equations represent the boundary integral equation for the induced stresses on the fracture surface and reservoir rocks, which can be numerically integrated with appropriate initial and boundary conditions. The above equations represent the boundary integral equation for the induced stresses on the fracture surface and reservoir rocks, which can be numerically integrated with appropriate initial and boundary conditions. The discretized form of the stress boundary integral equation can be written as (Vandamme and Curran, 1989; Kumar and Ghassemi, 2016):

$$\sigma_{ij}(\mathbf{x}) = \sum_{e=1}^{M} \int_A e \left\{ S_{ijkn}(\mathbf{x}, \mathbf{x'}) \cdot \sum_{m=1}^{N} \varphi^{(m)} D_{kn}^{(m)}(\mathbf{x'}) \right\} dA(\mathbf{x'}) + \sigma_{ij}^{0}(\mathbf{x}); \qquad (i, j, k, n = 1, 2, 3) \tag{3}$$

where e is the index for the element number, M is the total number of elements on the discretized fracture surface (s) or in the reservoir volume, m represents the node number, N is the number of nodes in an element, φ represents the interpolation shape functions, and σ_{ij}^{0} are the in-situ stress components. For numerical implementation, only the fracture surface discretization is required. Once, the DD's on the fracture surface are determined, the stresses and displacements in the reservoir can be estimated using Eq. (3).

2.2. Fluid Flow inside the Fractures

The fluid flow inside the fracture is described by Navier-Stokes' equation (Batchelor, 1967). Based on assumptions that the fracture aperture is of smaller magnitude than fracture length and varies smoothly, the lubrication theory is applicable for the hydraulic fracture fluid flow, which can be describe using "cubic law". The momentum balance for the fluid flow can be given in terms of pressure inside the fracture as (Witherspoon et al., 1980):

$$\mathbf{q} = -\frac{w^3}{12\mu}(\nabla p + \rho g \nabla z) \tag{4}$$

where $\mathbf{q}$ represents the fluid flux or fluid volume per unit area, w is the fracture width, p is the fluid pressure inside the fracture, μ is the fluid viscosity, ρ is the fluid density, and g represents the gravitational coefficient. For an incompressible fluid, the continuity equation can be written as (Yew, 1997):

$$\nabla \cdot \mathbf{q} = -\frac{\partial w}{\partial t} + -q_L + \delta(\mathbf{x} - \mathbf{x}_i) Q_i \tag{5}$$

where $\partial w / \partial t$ represent the rate of fracture volume change and q_L is the fluid leak-off rate from the one side of fracture surface into reservoir matrix, δ represents the Dirac delta function, and Q_i and $\mathbf{X_i}$ are the fluid injection rate and coordinates of the injection well, respectively. The pressure dependent fluid leak-off model is used in this study. Substitution of Eq. (4) into Eq. (5) results in the governing equation for fluid flow inside a fracture given as:

$$\frac{\partial}{\partial x}\left\{\frac{w^3}{12\mu}\frac{\partial p}{\partial x}\right\} + \frac{\partial}{\partial y}\left\{\frac{w^3}{12\mu}\left(\frac{\partial p}{\partial y} + \rho \mathbf{g}\right)\right\} = -\frac{\partial w}{\partial t} - 2q_L + \delta(\mathbf{x} - \mathbf{x}_i) Q_i \tag{6}$$

The above equation is subjected to boundary conditions as: the fluid flux at the wellbore must be equal to injection rate, whereas the fluid flux at the fracture front must be equal to zero or a "no-flow" boundary condition at the fracture front as (Ghassemi et al., 2013; Kumar and Ghassemi, 2016).The global mass balance conditions, which implies that the injection rate at which fracturing fluid is injected into fracture must be equal to the summation of the fracture volume change at any time and the fluid volume leak-off into the formation, is used to insure a unique solution of Eq.(6).

2.3. Proppant Transport and Deposition

The proppant transport within a hydraulic fracture is usually simulated by considering slurry a mixture of proppant particles and the fracturing fluid as a slurry. The proppant mass conservation condition inside a hydraulic fracture is given as (Pearson, 1994; Yew, 1997):

$$\frac{\partial (cw)}{\partial t} + \nabla \cdot \left(cw \mathbf{v}^P\right) = 0 \tag{7}$$

where c is the proppant volumetric fraction which is a ratio of the proppant volume (Vp) and the slurry volume (V), the $\mathbf{v}^P$ is the proppant velocity defined as (Novonty, 1977):

$$\mathbf{v}^P = \mathbf{v}^s + \mathbf{v}^{stl} \tag{8}$$

where $\mathbf{v}^s$ is the slurry velocity and $\mathbf{v}^{stl}$ is the proppant settling velocity. The proppant settling is implemented using a corrected Stokes velocity (Novonty, 1977) and its detailed implemented methodology can be found in Kumar et al. (2019). The proppant transport Eq. (7) is subjected to initial and boundary conditions. Initially whole fracture has zero proppant concentration i.e., $c(x, 0, z, 0) = 0$, during slurry injection the proppant concentration at the injection well is prescribed $c(0,0,0,t) = C_{inj}$, and a "no proppant flow" boundary condition at the fracture front is applied.

3. NUMERICAL METHODOLOGY

The 3D numerical model "GeoFrac-3D" is developed using a combination of displacement discontinuity method for the hydro-mechanical response of the fracture and reservoir rocks and the finite element method for the fracture fluid flow. The point collocation technique is used for the numerical implementation of boundary integral equation (i.e., Eq.3) (Zhou and Ghassemi, 2011; Ghassemi et al., 2013; Safari and Ghassemi, 2016; Kumar and Ghassemi, 2016). The Galerkin's finite element is used for the numerical modeling of the fracture fluid flow Eq. (6) (Smith and Griffiths, 1998; Zienkiewicz and Taylor, 2000). Details of the numerical implementation of Eqs. (3) & (6) and their coupled solution procedure can be found in Ghassemi et al. (2013) and Kumar and Ghassemi (2016 and 2018). The fracture propagation process is analyzed in the framework of the linear elastic fracture mechanics (LEFM). The modified 3D maximum circumferential criterion as suggested by Schöllmann et al. (2002) is used for the mixed-mode fracture propagation analysis and the fracture propagation growth is determined using scaling as suggested by Mastrojannis et al. (1980) and implemented in Kumar and Ghassemi (2016 and 2018). The proppant flow and transport within the fracture is modeled by representing the slurry as a mixture of fluid and proppant particles and is simulated using the finite element method (Kumar et al., 2019).

4. RESERVOIR ROCK PROPERTIES AND IN-SITU STRESSES

The "GeoFrac-3D" model used in this work has been verified previously by Zhou and Ghassemi (2011) and Ghassemi et al. (2013) and fracture propagation model is verified by Kumar and Ghassemi (2015). In this work, we have focused on the reservoir stimulation for the DOE's FORGE Utah EGS site as shown in Fig. 1. The objective of hydraulic fracturing is to generate a surface area more than 1000 m^2 to provide adequate heat exchange area for a production rate of about 50 liters/s at 170-200°C. The FORGE site is located 350 km south of Salt Lake City and 16 km north northeast of Milford, Utah, in an area that is predominantly used for renewable energy (i.e., wind, solar and geothermal) production. The rocks consist of basin fill sediments and crystalline basement rocks; the latter is mostly consisting of Miocene granitoids (Allis et al., 2016; Simmons et al., 2018) that will host the proposed EGS reservoir (see, Fig. 1). The reservoir rock physical properties and in-situ stresses are listed in Table 1. The experimental rock mechanics testing indicates crystalline basement rocks are very strong, and they have very low porosity (i.e., 0.13%) and very low permeability (i.e., 0.3 md) (Janis, 2018). The in-situ stress state of the FORGE site is in the normal faulting regime. The in-situ reservoir pressure and stresses distributions and well locations are shown in the Figs.2a, 2b, 2c, and 2d, respectively. The maximum horizontal principal stress (σ_H) is orientated N-E (Trend: N 25° E) and the minimum horizontal principal stress (σ_h) trend is N 125° E. The reservoir temperature is in the range of 175-225°C. During phase 2 of the Utah FORGE project, the Well 58-32 (see, Fig.2) was drilled and completed. The main purposes of drilling Well 58-32 is to directly measure reservoir properties including temperature, rock type, permeability, and reservoir stresses. In third phase of the project, an injection and production well doubt will be developed and used for the EGS research purpose. In study, we present analysis of hydraulic stimulation of the different potential of the Phase 3 wells; as three proposed inclined wells (as shown in Fig. 2) 3-1a and 3-1b (i.e., inclined well drilled parallel to the minimum horizontal stress direction), and Well 3-1c (i.e., inclined well drilled with an angle from the minimum horizontal stress direction).

Table 1. Reservoir rock properties and in-situ stresses for the FORGE Utah EGS site.

Parameter	Value
Reservoir rock type	Granitoid
Formation depth (h)	2361 (m)
Young's modulus (E)	58 (GPa)
Poisson's ratio (ν)	0.27
Vertical in-situ stress (σ_V) gradient	0.0254 (MPa/m)
Maximum horizontal stress (σ_H) gradient	0.0143 (MPa/m)
Minimum horizontal stress (σ_h) gradient	0.0138 (MPa/m)
Reservoir pore pressure gradient	0.0098 (MPa/m)
Rock toughness (K_{IC})	2.48 (MPa.$m^{0.5}$)
Thermal diffusivity (c)	9.71*10^{-7} (m^2/s)
Natural fracture density (NE/SW)	0.95 (fractures/m)
Natural fracture density (N/S)	0.36 (fractures/m)

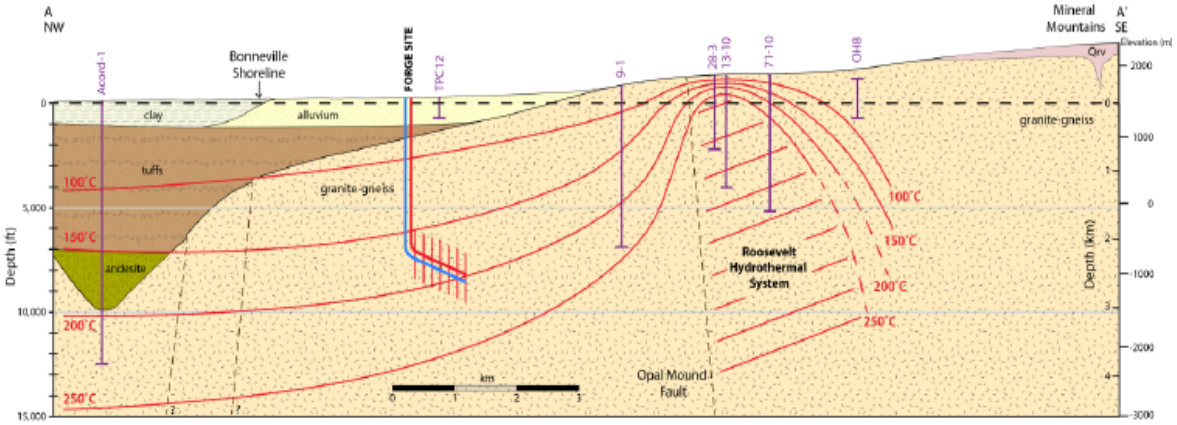

Figure 1. Geological cross-section of the FORGE Utah site showing the stratigraphy, structure, and thermal regime (Allis et al., 2016). Dark "blue and red" lines show the proposed Injection and Production well locations.

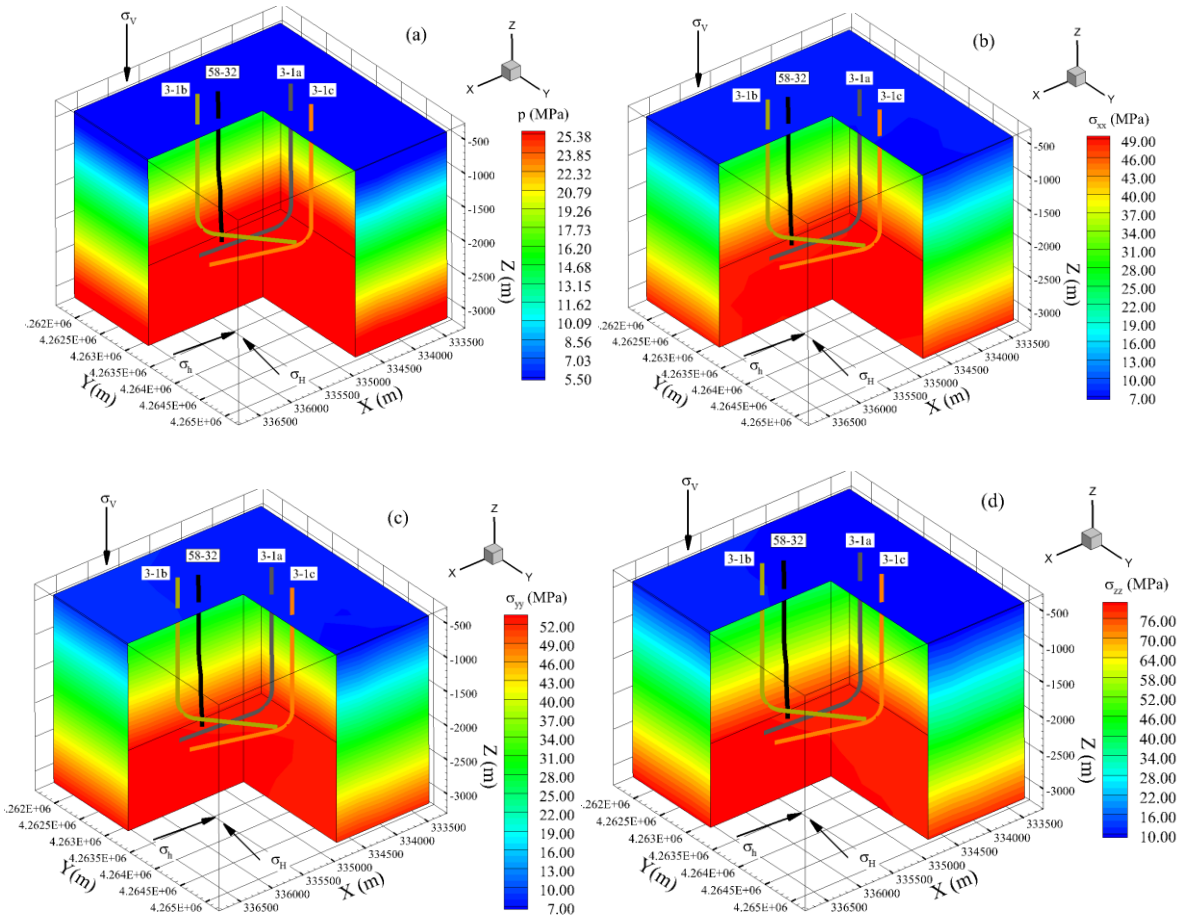

Figure 2. The orientation of the wells and distributions of the in-situ; (a) reservoir pore pressure, (b) the stress component σ_{xx}, (c) the stress component σ_{yy}, and (d) the vertical stress σ_{zz}. The in-situ stresses and pore pressure are varying with the formation depth.

5. SIMULATION EXAMPLES

5.1. A Fracture Propagation from the Well 3-1a or Well 3-1b and Well 3-1c

For the first example, numerical simulations of single fracture propagation from the proposed well 3-1a or well 3-1b is considered. As both the well 3-1a and well-3b are parallel to the minimum horizontal stress direction; hence, only results of the hydraulic stimulation of the well 3-1a are presented here. The initial perforation is assumed of radial shape with 1 (m) radius and perpendicular to the wellbore axis and is located at the "Toe" of the well coordinates X=335635.48 m, Y= 4262977.58 m, Z= -2361.074. To account for the presence of the natural fracture equivalent reservoir permeability is estimated as suggested by van Golf-Racht (1982). The fluid injection rate is taken equal to 37.5 bbl/min and fluid viscosity is equal to 1 cP. As the initial perforation is align in the preferred fracture propagation path (i.e., along σ_H direction). The fracture in this case shows planar propagation. However, due to the in-situ gradient variation with formation depth, it experiences relatively lower stresses or resistance for propagation in the upward direction; hence, more growth in the upward direction is observed as shown in Fig. 3a. A time variation of the fracture width at wellbore, fracture upward growth, and the net injection pressure are shown in Figs. 3b, 3c, and 3d, respectively.

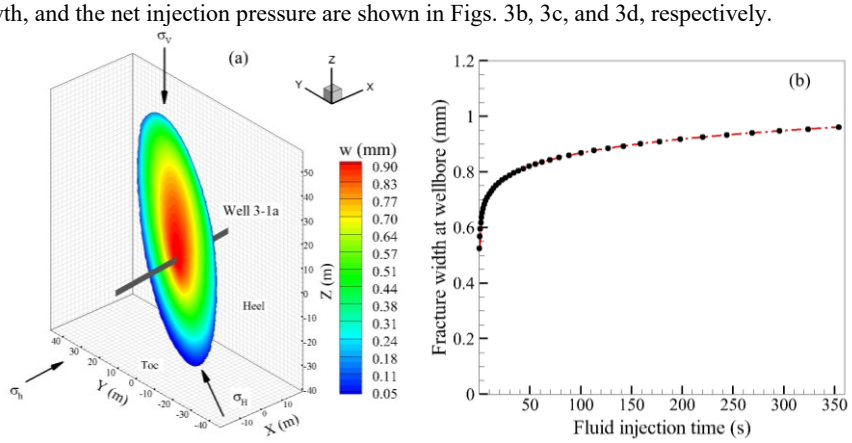

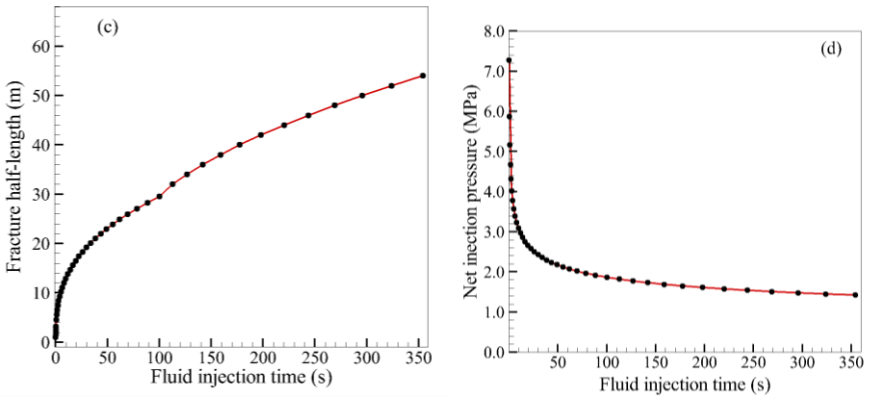

Figure 3. (a) Distribution of fracture apertures, and time variation of; (b) fracture width at wellbore, (c) fracture upward growth and (d) the net injection pressure for the well 3-1a.

For the second example, consider the numerical simulations of single fracture propagation from the proposed well 3-1c, which deviated by 20° form the minimum horizontal stress direction. The fluid injection rate is taken equal to 37.5 bbl/min and fluid viscosity is equal to 1 cP. The initial perforation is assumed of circular shape with 1 (m) radius and perpendicular to the wellbore axis. As the initial perforation is not align in the preferred fracture propagation path (i.e., along σ_H direction). The fracture in this shows non-planar propagation, which eventually tend to align with the maximum horizontal stress direction as shown in Fig. 4a. A time variation of the fracture width at wellbore, fracture upward growth, and the net injection pressure are shown in Figs. 3b, 3c, and 3d, respectively. It is observed that in this due to near wellbore tortuosity effect, significant higher injection pressure is need to start fracture propagation as compared to previous planar fracture case (see, Fig.3d and 4d).

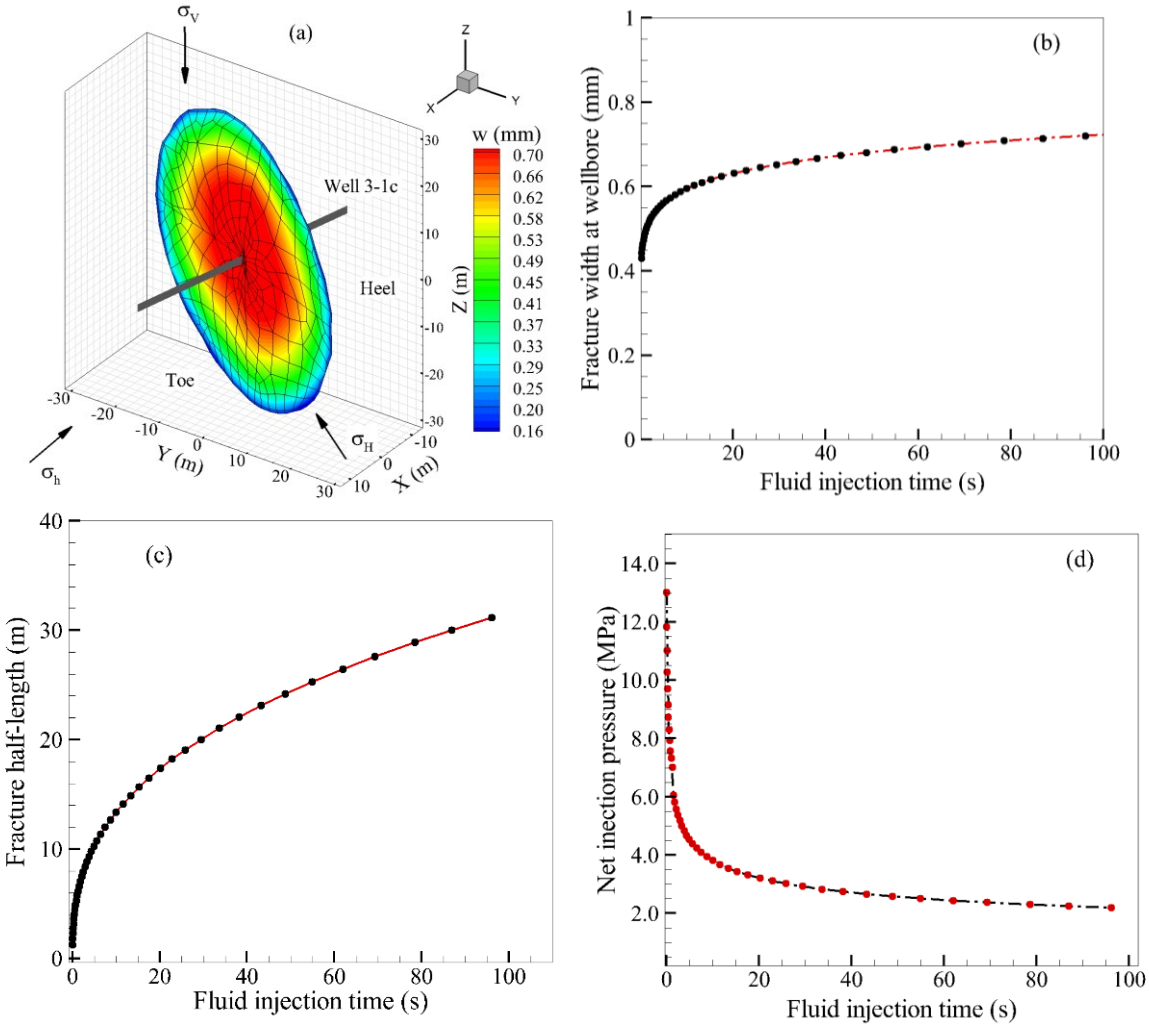

Figure 4. (a) Distribution of fracture apertures, and time variation of; (b) fracture width at wellbore, (b) fracture upward growth and (d) the net injection pressure for the well 3-1c.

5.2 Simulation of Proposed FORGE Utah EGS Doublet System

In this section, we present numerical example of the hydraulic stimulation of the proposed EGS doublet system for the FORGE Utah site. A schematic of the proposed EGS doublet system is shown in Fig. 5, where the wells are inclined by 60° from the vertical direction (i.e., from z-axis in this case) and the wells are aligned with the minimum horizontal stress (σ_h) direction. The initial perforations are aligned with the maximum horizontal stress (σ_H) direction and are parallel to the YZ plane. As a first example, consider the simultaneous multistage fracturing of a horizontal and an inclined well. This simulation demonstrates the case, where only the production well is stimulated. The reservoir physical properties and in-situ stress condition are the same as in Table 1. The fluid injection rate per stage is assumed constant and is equal to 0.1 m^3/s (37.5 bbl/min). The fracturing fluid used is water with fluid viscosity of 0.001 Pa.s (1 cp). The spacing between wells is 75 (m) and stage spacing is equal to 50 (m). Results of the two, single cluster stages (having only one dominating fracture in each cluster) are shown in Figure 7 for a horizontal well and an inclined well. It is important to mention here that in the case of simultaneous fracturing; nonplanar propagation of the fractures may occur. However, we have used a sufficiently large spacing so that planar fracture propagation is observed. Note that fractures in both cases are showing upward growth and they eventually intersect with the production well and provide connectivity between the production and injection wells for the water circulation. The stage-2 fracture in the inclined well is in a lower stress zones (due to stress gradient) and shows more upward growth. For the same injection parameters, the fractures from the inclined well (Fig.6b) are showing slightly higher fracture apertures as compared to the horizontal well fracture (Fig.6a), which is due to relatively lower overlapped region and lower stresses on the fracture surfaces. The results in this case demonstrate that for better heat energy recovery the inclination angles of the wells should be minimized. Since, for the inclined wellbore case, the "Heel" side fractures (i.e., Stage-2 fracture in Fig.6b) will be in relatively lower temperature zones. The input parameters for the proppant transport and deposition simulation are listed in Table 2. The proppant concentration distribution at the end of fluid injection for the horizontal and inclined well cases are shown in Fig.7a and 7b, respectively. It is observed that in both the cases the proppants have a downward settling tendency and about 55% of the fracture area is effectively propped.

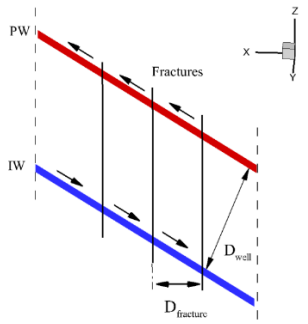

Figure 5. Schematics of the proposed inclined EGS doublet system with multiple fractures (redrawn after Asai et al., 2018). PW: Production well, IW: Injection well. The wells inclination angle from the vertical direction is equal to 60°.

Table 2. Input parameters for the proppant flow simulation.

Parameter	Value
Proppant material	Sintered Bauxite
Proppant size	40/80 mesh size
Proppant diameter	330 µm
Material specific gravity	3.3
Bulk density	1970 kg/m^3
Proppant injection rate	6.93 ppg (c = 0.2)

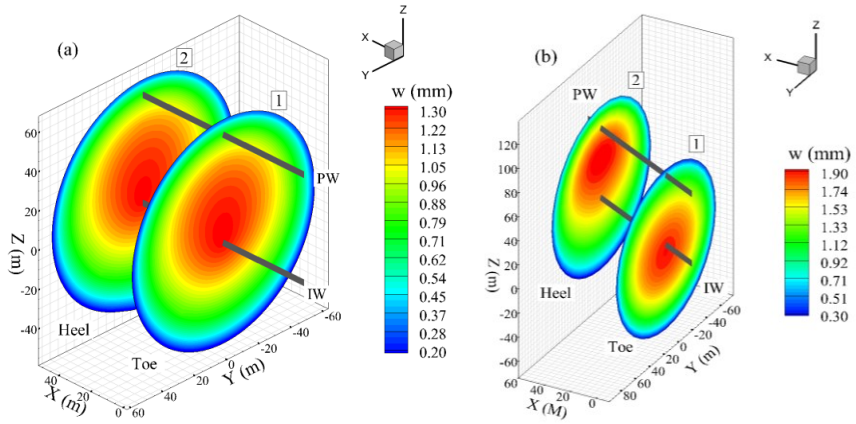

Figure 6. Distribution of fracture opening and generated fracture network: (a) simultaneous fracturing of a horizontal well and (b) simultaneous fracturing of an inclined well (total contact surface area = 29086.67 m^2).

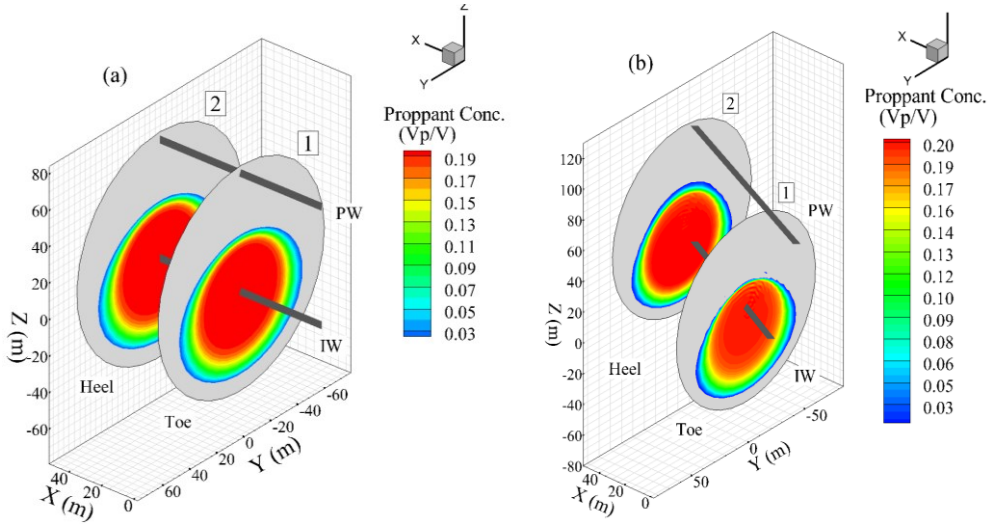

Figure 7. Proppant distribution at end of fluid injection; (a) simultaneous fracturing of a horizontal well (effective area = 16,114 m^2, propped area = 55.4%) and (b) simultaneous fracturing of an inclined well (effective propped area = 16,021.4 m^2, propped area = 55%).

The impact of fracturing fluid density is investigated in this case and a comparison of the results of the fracture geometries and fracture aperture for the water and higher density fracturing fluid are shown in Figs. 8. It is observed that fracturing fluid density has impacts the fracture growth pattern. A higher density fracturing fluid due to more gravitational impact promotes downward growth of the fractures. The results demonstrate that the unwanted upward growth of the fractures in the EGS reservoir can be mitigated by using higher density fracturing fluids.

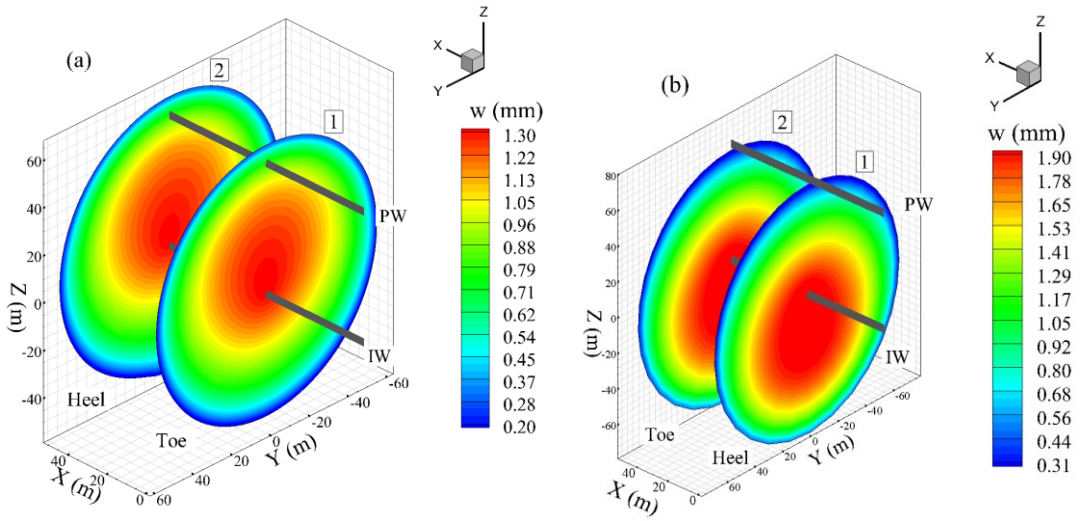

Figure 8. Impact of the fracturing fluid density on the fracture growth tendency: (a) water (fluid density = 1000 km/m^3, fluid viscosity = 0.001 Pa.s), (b) higher density fluid (fluid density = 1250 kg/m^3, fluid viscosity = 0.005 Pa.s). The higher density fluid promotes downward growth of the fractures.

For the second example, consider the conventional simultaneous zipper fracturing of two inclined wells. In this case, the multiple wells are stimulated at the same time and fractures from those wells propagate towards each other. In this study, it is assumed that each stage contains one fracture cluster with only one dominating fracture. The fluid injection rate is assumed constant and is equal to 0.1 m^3/s (37.5 bbl/min) for both the horizontal wells. The fracturing fluid used is water with fluid viscosity of 0.001 Pa.s (1 cp). The spacing between wells is 100 (m) and stage spacing is equal to 50 (m). Results of a single stage per well (with one fracture cluster having only one dominating fracture) are shown in Fig.9a. It is observed that fractures from both wells show upward growth and so the lower well fractures may eventually intersect the upper well The results in this case demonstrate that for better stimulation efficiency and well connectivity, the zipper fracturing might be the preferred technique over the simultaneous fracturing of only the production well. Since, both the conventional and modified zipper fracturing simulations have shown strong potential for wells connectivities though fracture-to-fracture interference. Additionally, in the zipper fracturing technique relatively a lesser propagation of fractures will provide the needed connectivity between the wells. For example, if the spacing between the wells is 100 (m) then only 50 (m) propagation of fractures from each well will show the possibility of coalescence of their tips and hence, the wells connectively. Whereas, in case of only fracturing the production well, to ensure wells connectivity the fractures have to propagate at least 100 (m). The proppant concentration distribution at the end of fluid injection is shown in Fig.9b. It is observed the proppant is showing downward settling tendency and about 52.1% of the fracture area is effectively propped.

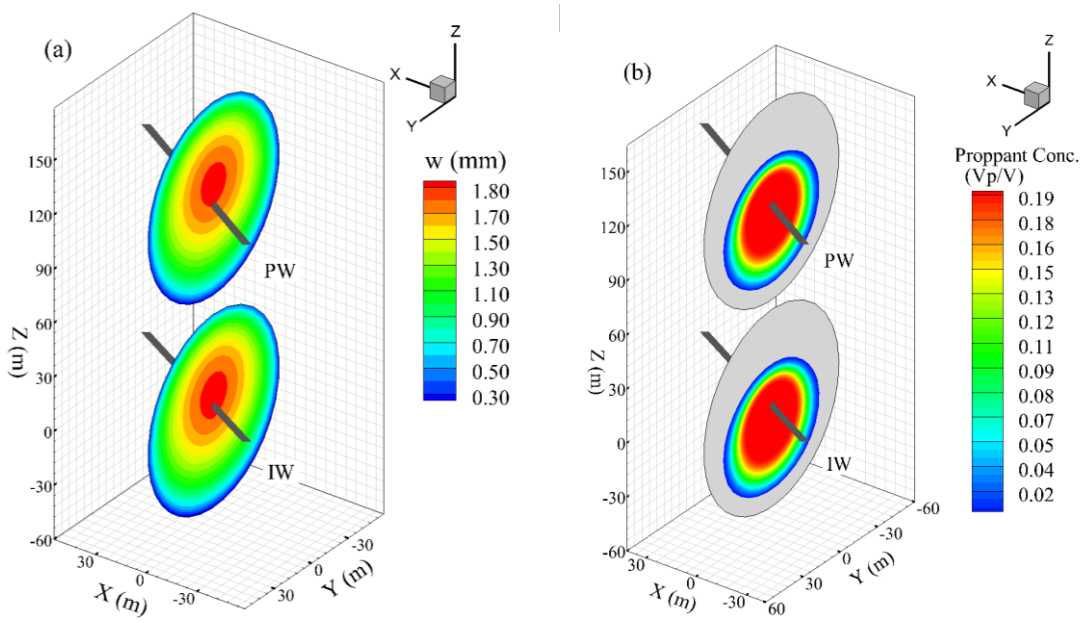

Figure 9. Results of conventional simultaneous zipper fracturing of an inclined well: (a) distribution of fracture openings, (b) Proppant distribution at end of fluid injection (total contact surface area =17843.6 m^2, effective propped area =9296.51 m^2, propped area =52.1%).

5.3 Simultaneous Zipper Fracturing of Horizontal Wells

In this section, numerical simulations of multiple transverse fracture clusters are presented. The multiple horizontal well fracturing can be done either using conventional zipper fracturing or modified zipper fracturing (Sesetty and Ghassemi, 2015; Kumar and Ghassemi, 2016). The horizontal well is aligned with the minimum horizontal in-situ stress (σ_h) and initial perforation are orthogonal to the wellbore axis and aligned with the maximum horizontal in-situ stress (σ_H). As mentioned earlier, to avoid the thermal interference among fractures, the spacing among stages is set equal to 50 (m), which corresponds to the thermal diffusion distance for 20 years of production. The spacing between the lateral wells is set equal to 100 (m). The stimulation process starts from the wellbore "toe" to "heel" and is carried-out in multiple stages. For the first example, consider the conventional simultaneous zipper fracturing of two horizontal wells at the same reservoir depth. In this case, the multiple wells are stimulated at the same time and fractures from those wells propagate towards each other. In this study, it is assumed that each stage contains one fracture cluster with only one dominating fracture. The reservoir physical properties and in-situ stress condition are the same as in Table 1. The fluid injection rate is assumed constant and is equal to 0.1 m^3/s (37.5 bbl/min) for both the horizontal wells. The fracturing fluid used is water with fluid viscosity of 0.001 Pa.s (1 cp). The created fracture network and distribution of the normal fracture openings after completion of the second stage fracturing are shown in Fig.10a. The first set of fractures (e.g., Stage-1 fractures) is created at the same time from the both horizontal wells. After completion of Stage-1 fracturing, the next set of simultaneous fractures (e.g., Stage-2 fractures) is created while keeping the Stage-1 fractures pressurized. The assumption of the constant pressure in previously created fractures, restricts the flow-back from these fractures due to creation of the next stage fractures. This constant pressure is assumed equal to average value of the Stage-1 fluid pressure in the last time step of their propagation. The side view of the propagated fracture geometries and induced stress shadowing (i.e., increase of stress component $\Delta\sigma_{xx}$) are shown in Fig.10b. The "dotted lines" show the local maximum principal stress plot in the central XY plane (Fig.10b). It can be observed that the fractures tips are align in the direction of the maximum local principal stresses. The creation of factures without an initial offset between stages induces symmetric compressive (see, Stage-1 part in Fig.10b) and shear stresses around the fractures which cancel out and keep the fracture propagation planar as shown in Stage-1 part of Fig.10b. However, during creation of Stage-2 fractures, the Stage-1 fractures induce stress shadowing effects which alters the principal stress directions (see, Fig.10b) for the subsequent fracturing stages. Hence, the resultant fractures are slightly deviated from the vertical plane. The subsequent fracturing stages tend to induce a closure on the previously created stage fractures due to induced compressive stresses. Hence, Stage-1 and Stage-2 fractures in Fig.10b shows less opening compared to Stage-2 fractures. The final fracture network has a total contact surface area equal to 31415.9 m^2. From Fig.10b, it can be observed that if we continue the fracturing process, the fractures from both wells will tend to merge and will provide connectivity between the wells for water circulation.

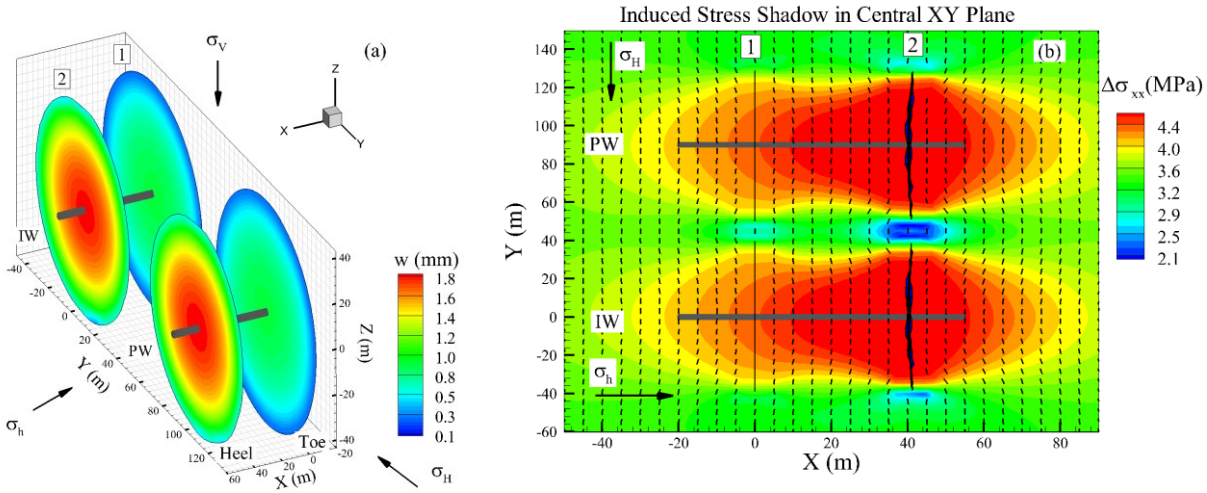

Figure 10. Results of conventional simultaneous zipper fracturing: (a) distribution of fracture opening, (b) side-view of fracture network and induced stress shadow (total contact surface area = 31415.9 m^2).

For the second example, consider the modified simultaneous zipper fracturing of two parallel horizontal wells at the same reservoir depth. In modified simultaneous zipper fracturing, the multiple wells are stimulated at the same time with an initial offset between stages from two wells. In this case, the offset between two fractures of a particular stage are kept equal to 15 (m). The total fluid injection rate is constant and is equal to 0.1 m^3/s (37.5 bbl/min) for both the horizontal wells (water with fluid viscosity of 1 cp). The first set of fractures (Stage-1) is created at the same time in both horizontal wells with an initial offset. In Stage-2, the next set of simultaneous fractures is created while the Stage-1 fractures are kept pressurized. The created fracture network and distribution of the normal fracture openings after completion of the second stage of fracturing is shown in Fig.11a. The side-view of the propagated fracture geometries, induced stress shadow, and trajectories of the local maximum principal stresses are shown in Fig.5b. It is observed that in this case, the fractures propagating from each horizontal well tend to turn towards one another, which is happening due to action of the induced stress fields near the fracture inner tips as shown in Fig.12b. During creation of Stage-2, the previous stage fractures induce a stress shadow (see, Fig.11b); hence, the resultant fractures deviate and curves as shown in Stage-2 of Fig.11a. It can be noticed that relatively high shear stresses are induced in between the inner tips of the fractures, which suggests that if we keep fracture propagation process, the inner tips of the fractures will tend to propagate toward each other for some distance before re-aligning themselves. The final fracture networks result in total surface contact area equal to 30787.6 m^2, which is slightly less than the previous scheme.

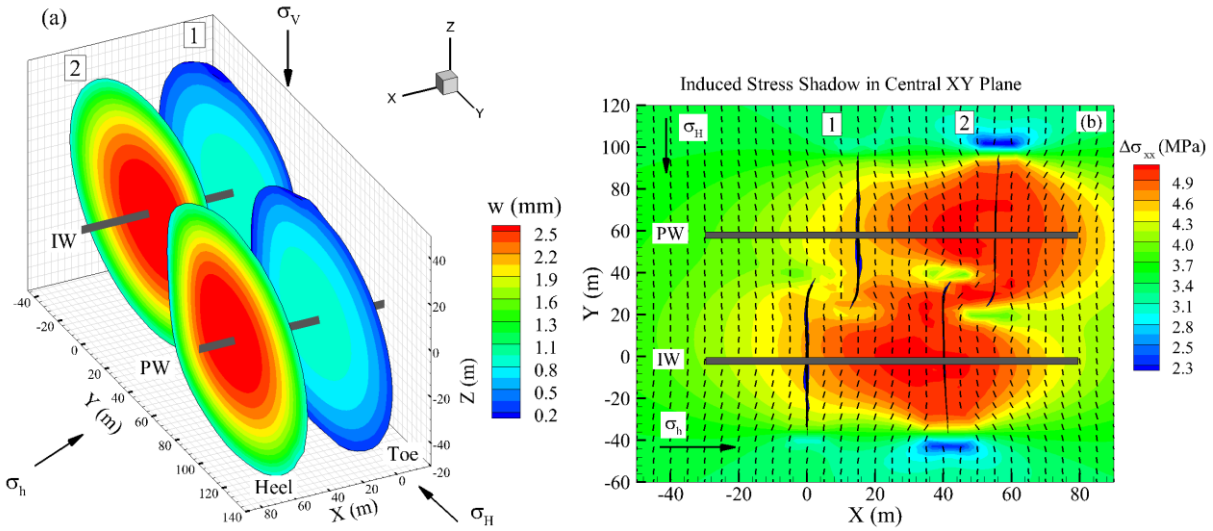

Figure 11. Results of modified simultaneous zipper fracturing: (a) distribution of fracture opening, (b) side view of fracture network and induced stress shadow (total surface contact area = 30787.6 m^2).

6. SUMMARY AND CONCLUSION

A numerical model "GeoFrac-3D" to simulate 3D hydraulic fracture propagation from the horizontal wells with capabilities to simulate multistage fracturing has been developed. The DD method for the solid and fracture deformation modeling presents a numerically and computationally efficient numerical scheme; since, boundary integral equations require only fracture surface discretization. The numerical examples of multiple horizontal wells simulation using conventional zipper fracturing and modified zipper fracturing are presented. It is observed that both the conventional and modified zipper fracturing shows the possibility of coalescence of their tips. However, the modified zipper fracturing generates more complex fracture network, which would result in enhancement of reservoir permeability. The results demonstrate that stresses shadowing effect, which mainly depends on the interval

between the fractures shows a strong influence on the simultaneous propagation of the multiple fractures. However, in the EGS, keeping the thermal diffusion distance as spacing between lateral wells and fractures reduces mechanical interaction among fractures. For better heat energy recovery, the inclination angles of the wells should be minimized. Fluid density can be manipulated to prevent excessive upward growth of the fracture and to promote downward growth.

ACKNOWLEDGEMENT

This material was based upon work supported by the Utah FORGE project sponsored by the U.S. Department of Energy, Office of Energy Efficiency and Renewable Energy (EERE), Office of Technology Development, Geothermal Technologies Office (GTO) and the OU Reservoir Geomechanics JIP.

REFERENCES

Allis, R.G., Moore, J.N., Davatzes, N., Gwynn, M., Hardwick, C., Kirby, S., Pankow, K., Potter, S., and Simmons, S.F. EGS Concept Testing and Development at the Milford, Utah FORGE Site. Proceedings, 41st Workshop on Geothermal Reservoir Engineering, Stanford University, Stanford, CA, USA, (2016).

Asai, P., Panja, P., MeLennan, J., and Moore, J. Performance evaluation of enhanced geothermal system (EGS): surrogate models, sensitivity study and ranking key parameters. Renewable Energy, Vol. 122 (2018), 184-195.

Batchelor, G.K.: An introduction to fluid dynamics. Cambridge University Press, Cambridge, UK, (1967).

Crouch, S.L., and Starfield, A.M. Boundary Element Methods in Solid Mechanics. London: George Allen & Unwin (1983).

Fan, Y., and Economides, M.J. Fracturing fluid leak-off and net pressure behavior in Frac&pack Stimulation. SPE-29988, International Meeting on Petroleum Engineering, Beijing, PR, China, (1995).

Ghassemi, A., Roegiers, J-C. A three-dimensional poroelastic hydraulic fracture simulator using the displacement discontinuity method. In: Proceedings of the 2nd North American rock mechanics symposium, Montreal, Canada (1996).

Ghassemi, A., Zhou, X., and Rawal, C. A three-dimensional poroelastic analysis of rock failure around a hydraulic fracture. J. of Petro. Sci. & Eng., Vol. 108 (2013),118-127.

Janis, M. 3D reservoir geomechanics model for the proposed FORGE laboratory site near Milford, Utah. MS Thesis, The University of Oklahoma, Norman, OK, USA (2018).

Kumar, D., and Ghassemi, A. 3D simulation of multiple fracture propagation from horizontal wells. 49th US Rock Mechanics/Geomechanics Symposium, Fan Francisco, CA, USA (2015).

Kumar, D. and Ghassemi, A. A three-dimensional analysis of simultaneous and sequential fracturing of horizontal wells. J. of Petrol. Sci. Eng., Vol.146 (2016), 1006-1025.

Kumar, D. and Ghassemi, A. A three-dimensional poroelastic modeling of multiple hydraulic fracture propagation from horizontal wells. Int. J. of Rock Mech. and Mining Sci., Vol.105 (2018), 192-209.

Kumar, D., Gonzalez, R.A., and Ghassemi, A. The role of micro-proppants conductive fracture network development. SPE Hydraulic Fracturing Conference and Exhibition, Woodlands, TX, USA (2019).

Mastrojannis, E.N., Keer, L.M., and Mura, T. Growth of planar cracks induced by hydraulic fracturing. Int. J. Numer. Methods Eng., Vol. 15(1) (1980), 41-54.

Novonty, E.J. 1977. Proppant Transport. 52nd SPE ACTE, Denver, CO, USA, (1977).

Pearson, J.R.A. On suspension transport in fracture: framework for a global model. J. Non-Newtonian Fluid Mech., Vol.54 (1994), 503-513.

Safari, R., and Ghassemi, A. Three-dimensional poroelastic modeling of injection induced permeability enhancement and micro-seismicity. Int. J. of Rock Mech. and Mining Sci., Vol. 84 (2016), 47-58.

Sesetty, V.K, and Ghassemi, A., Numerical simulation of sequential and simultaneous hydraulic fracturing. Intech: Effective and Sustainable Hydraulic Fracturing, (2013).

Sesetty, V.K., and Ghassemi, A. Modeling and analysis of sequential and simultaneous hydraulic fracturing in single and multi-lateral horizontal wells. Int. J. Petroleum Sci. and Eng., Vol. 132 (2015), 65-76.

Simmons, S.F., Moore, J., Allis, R., Kirby, S., Jones, C., Bartley, J., Kleber, E., Knudsen, T., Hardwick, C., Rahilly, K., Gwynn, M., MeLennan, J., Forbes, B., Podgorney, R., Pankow, K., Wannamaker, P., and Fischer, T. A revised geoscientific model for FORGE Utah EGS Laboratory. Proceedings, 43rd Workshop on Geothermal Reservoir Engineering, Stanford University, Stanford, CA (2018).

Smith, I.M., and Griffiths. D.V. Programming the finite element method. 3rd edition (1998), Wiley, Hoboken, New Jersey.

Schöllmann, M., Richard, H.A., Kullmer, G., and Fulland, M. A new criterion for the prediction of crack development in multi-axially loaded structures. Int. J. of Fract. Vol.117 (2002), 129-141.

Vandamme, L., and Curran, J.H. A three-dimensional hydraulic fracturing simulator. Int. J. Num. Method in Engg, Vol. 28 (1989), 909-927.

Van Golf-Racht, T.D. Fundamental of fracture reservoir engineering. Development in Petroleum Science, Vol. 12, Elsevier, 1982.

Waters, G.A., Barry, K.D., Robert, C.D., Kenneth, J.K., and Lance, A. Simultaneous hydraulic fracturing of adjacent horizontal wells in Woodford shale. SPE Hydraulic Fracturing Technology Conference, Woodlands, Texas, USA, (2009).

Wiles, T.D., and Curran, J.H. A general 3D displacement discontinuity method. Proceeding of 4th Int. Conference for Numerical Methodods in Geomech, (1982),103-111.

Witherspoon, P.A., Wang, J.S., Iwai, K., and Gale, J.E. Validity of cubic law for fluid flow in a deformable rock fracture. Technical Information Report No.23, University of California, Berkeley and Lawrence Berkeley Laboratory, (1979).

Yew, C.H. Mechanics of hydraulic fracturing. Gulf Publishing Company, Houston, Texas, USA (1997).

Zhou, X., and Ghassemi, A. Three dimensional poroelastic analysis of pressurized natural fracture. Int. J. Rock Mech. and Mining Sci., Vol. 48 (2011), 527-534.

Zienkiewicz, O.C., and Taylor, R.L. Finite element method. Col. 1, The Basis Butterworth-Heinemann, Amsterdam, (2000).